Computers and Mathematics with Applications 70 (2015) 548–561

Contents lists available at ScienceDirect

Computers and Mathematics with Applications

journal homepage: www.elsevier.com/locate/camwa

Lattice Boltzmann model for a class of convection–diffusion equations with variable coefficients

Qianhuan Li, Zhenhua Chai, Baochang Shi *

School of Mathematics and Statistics, Huazhong University of Science and Technology, Wuhan 430074, People's Republic of China

ARTICLE INFO

Article history:
Received 31 March 2014
Received in revised form 5 May 2015
Accepted 7 May 2015
Available online 4 June 2015

Keywords:
Lattice Boltzmann model
Convection–diffusion equation
Variable coefficients

ABSTRACT

In this work, a lattice Boltzmann model for a class of n-dimensional convection–diffusion equations with variable coefficients is proposed through introducing an auxiliary distribution function. The model can exactly recover the convection–diffusion equation without any assumptions. A detailed numerical study on several types of convection–diffusion equations is performed to validate the present model, and the results show that the accuracy of the present model is better than previous models.

1. Introduction

Partial differential equations (PDEs) play an important role in various fields, such as electricity, hydrodynamics, heat, magnetism, optics, elasticity and so on [1,2]. As an important kind of the second-order PDE, the convection–diffusion equation (CDE) can be used to describe numerous complex and interesting phenomena, caused by the convection and diffusion processes. Therefore, the studies on the solution of the CDE are of great importance in many fields of science and engineering. However, it may be very difficult to obtain an exact solution of the general CDE, especially for those with variable coefficients. On the contrary, the numerical methods, including finite-element method [3,4], finite-difference method [5,6], finite-volume method [7] can be served as an alternative to solve the CDE with the development of computer technology.

It is well known that the lattice Boltzmann method (LBM) has been successfully applied to study the complex fluid flows [8], such as microfluidics [9], multiphase/multicomponent flow [10,11], thermohydrodynamics [12], electro-osmotic flow [13], and so on. Compared with traditional computational methods, the LBM is intrinsically parallel, easy to program, and efficient to deal with complicated boundary conditions, and can be extended to high-dimensional problems. Besides, LBM can also be used to solve nonlinear systems, described by the reaction–diffusion equation [14], CDE [15–19] and high-order PDE [20].

Up to the present, most of the existing lattice Boltzmann (LB) models are only limited to the CDEs with variable coefficient in the diffusion term, while the CDEs with variable coefficients in the convection term are still seldom considered. We note that the model in Ref. [21] can be used to solve the Fokker–Planck equation (FPE), which is a special case of CDE with variable coefficients, but it contains some assumptions (see Remark 4 in Section 2). Actually, the CDE with variable coefficients has many applications, including hydro-dynamic dispersion process, pollution control, soil physics, bio-physics, petroleum engineering and chemical engineering. Therefore, developing a LB model for the CDE with variable coefficients is of great significance. In this paper, a new LB model, as an extension of our model in Ref. [16], is proposed for the CDE with variable

* Corresponding author.
E-mail address: shibc@hust.edu.cn (B. Shi).

http://dx.doi.org/10.1016/j.camwa.2015.05.008
0898-1221/

coefficients through introducing auxiliary distribution function. Similar to Ref. [15], the present model also introduces a source term when it is used to study the CDE with variable coefficients in convection term.

The rest of the paper is organized as follows. In Section 2, a lattice Bhatnagar–Gross–Krook (LBGK) model for the CDE with variable coefficients is proposed and some of its special cases are discussed. In Section 3, some numerical tests are performed to test the present model, and finally, a brief summary is given in Section 4.

2. The LBGK model for CDE with variable coefficients

The n-dimensional (nD) CDE with variable coefficients and a source term can be written in the following form,

$$\partial_t \phi + \nabla \cdot [a(\phi)\mathbf{U}(\mathbf{x}, t)] = \nabla \cdot [\alpha(\mathbf{x}, t)\nabla \cdot \mathbf{D}(\mathbf{x}, t, \phi)] + F(\mathbf{x}, t, \phi), \tag{1}$$

where ∇ is the gradient operator with respect to the position $\mathbf{x}$ in n dimensions. $a(\phi)\mathbf{U}(\mathbf{x}, t)$ is the convection term, $a(\phi)$ is a known function of ϕ, which is an unknown real/complex-valued scalar function of position $\mathbf{x}$ and time t, $\mathbf{U}(\mathbf{x}, t)$ is the vector function. $\mathbf{D}(\mathbf{x}, t, \phi)$ is the diffusion term and related to spatial coordinate $\mathbf{x}$, time t and ϕ. $\alpha(\mathbf{x}, t)$ and $F(\mathbf{x}, t, \phi)$ are the diffusion coefficient and source term, respectively.

In this work, the LBGK model is considered for its simplicity and efficiency in the study of the fluid flows and nonlinear PDEs. The evolution equation of the LBGK model reads

$$\begin{aligned} f_i(\mathbf{x} + \mathbf{c}_i\Delta t, t + \Delta t) - f_i(\mathbf{x}, t) = & -\frac{1}{\tau}[f_i(\mathbf{x}, t) - f_i^{eq}(\mathbf{x}, t)] + \Delta t[F_i(\mathbf{x}, t) + G_i(\mathbf{x}, t)] \\ & + (\Delta t)^2\partial_t F_i(\mathbf{x}, t)/2, \quad i = 0, \ldots, q-1, \end{aligned} \tag{2}$$

where $\mathbf{c}_i = c\mathbf{e}_i$ is the set of possible discrete velocity directions, c is particle velocity and defined by $c = \Delta x/\Delta t$ with Δx and Δt representing the discrete steps of space and time, respectively. τ is the dimensionless relaxation time, $f_i(\mathbf{x}, t)$ and $f_i^{eq}(\mathbf{x}, t)$ are the local distribution function and its equilibrium part. $F_i(\mathbf{x}, t)$ and $G_i(\mathbf{x}, t)$ are the distribution functions of the source and convection term with variable coefficient, respectively.

Similar to Ref. [16], our model is based on the DnQq lattice (q is the number of velocity directions in n-dimensional space), and the distribution functions of equilibrium part and source term can be written as

$$\begin{aligned} f_i^{eq} &= \omega_i\left[\phi + \frac{\mathbf{c}_i \cdot (a\mathbf{U})}{c_s^2} + \frac{(\mathbf{C} + c_s^2\beta\mathbf{D} - c_s^2\phi\mathbf{I}) : (\mathbf{c}_i\mathbf{c}_i - c_s^2\mathbf{I})}{2c_s^4}\right], \\ F_i &= \omega_i F\left[1 + \lambda\frac{\mathbf{c}_i \cdot (a'\mathbf{U})}{c_s^2}\right], \end{aligned} \tag{3}$$

where $a' = \frac{da}{d\phi}$, $\mathbf{C}$ is an auxiliary moment [16], and defined by $\mathbf{C} = \mathbf{UU}\int a'a'd\phi$, β is a parameter used to adjust the dimensionless relaxation time τ as in Ref. [19]. $\mathbf{I}$ is the unit matrix, and $\lambda = 1 - \frac{1}{2\tau}$. c_s is the so-called sound speed, which is related to the particle velocity c and weight coefficients ω_i through $\sum_i \omega_i\mathbf{c}_i\mathbf{c}_i = c_s^2\mathbf{I}$. Here some commonly used DnQq models are listed in Table 1.

In order to recover Eq. (1) exactly, besides the above distribution functions, an auxiliary distribution function is also introduced, and defined by

$$G_i = \omega_i\lambda\frac{\mathbf{c}_i \cdot \mathbf{S}}{c_s^2}, \tag{4}$$

where $\mathbf{S} = a\partial_t\mathbf{U} - aa'\mathbf{U}\nabla \cdot \mathbf{U} + \int a'a'd\phi\nabla \cdot (\mathbf{UU})$. When U is a known analytic function, one can directly calculate the gradients in $\mathbf{S}$. On the other hand, if U is unknown, $\mathbf{S}$ can be computed by some finite-difference schemes. Here we would like to point out that we can also use the idea of the model in Ref. [15] to treat the convective term $a\mathbf{U}$. To recover the correct CDE with variable coefficients, above distribution functions should satisfy the following relations:

$$\sum_i f_i = \sum_i f_i^{eq} = \phi, \qquad \sum_i \mathbf{c}_i f_i^{eq} = a\mathbf{U}, \qquad \sum_i \mathbf{c}_i\mathbf{c}_i f_i^{eq} = c_s^2\beta\mathbf{D} + \mathbf{C}, \tag{5}$$

$$\sum_i F_i = F, \qquad \sum_i \mathbf{c}_i F_i = \lambda a'\mathbf{U}F, \tag{6}$$

$$\sum_i G_i = 0, \qquad \sum_i \mathbf{c}_i G_i = \lambda\mathbf{S}. \tag{7}$$

In what follows, we will present a detailed Chapman–Enskog analysis to derive Eq. (1). Following the work of [16], the distribution function, the source term, and the derivatives of space and time can be expanded as

$$\begin{aligned} & f_i = f_i^{(0)} + \epsilon f_i^{(1)} + \epsilon^2 f_i^{(2)} + \epsilon^3 f_i^{(3)} + \cdots, \\ & F = \epsilon F^{(1)}, \qquad G = \epsilon G^{(1)} + \epsilon^2 G^{(2)}, \\ & \partial_t = \epsilon\partial_{t_1} + \epsilon^2\partial_{t_2}, \qquad \nabla = \epsilon\nabla_1, \end{aligned} \tag{8}$$

Table 1
The discrete velocity directions and corresponding weight coefficients of D*n*Q*q*.

D*n*Q*q*	$\mathbf{e}_i$	ω_i
D1Q3	(0), (±1)	2/3, 1/6
D2Q9	(0, 0), (±1, 0), (0, ±1), (±1, ±1)	4/9, 1/9, 1/9, 1/36
D3Q15	(0, 0, 0), (±1, 0, 0), (0, ±1, 0), (0, 0, ±1), (±1, ±1, ±1)	2/9, 1/9, 1/9, 1/9, 1/72
D3Q19	(0, 0, 0), (±1, 0, 0), (0, ±1, 0), (0, 0, ±1), (±1, ±1, 0), (±1, 0, ±1), (0, ±1, ±1)	1/3, 1/18, 1/18, 1/18, 1/36, 1/36, 1/36

where ϵ is a small parameter. Taking the Taylor series expansion of Eq. (2) at time t and space $\mathbf{x}$, we have

$$\triangle t D_i f_i + \frac{\triangle t^2}{2} D_i^2 f_i + \cdots = -\frac{1}{\tau}(f_i - f_i^{eq}) + \triangle t(F_i + G_i + \triangle t \partial_t F_i/2), \tag{9}$$

where $D_i = \epsilon D_{1i} + \epsilon^2 \partial_{t_2}$ and $D_{1i} = \partial_{t_1} + \mathbf{c}_i \cdot \nabla_1$. Substituting Eq. (8) into Eq. (9), we can obtain the following equation,

$$\begin{aligned}&(\epsilon^2\partial_{t_2} + \epsilon D_{1i})(f_i^{(0)} + \epsilon f_i^{(1)} + \epsilon^2 f_i^{(2)} + \cdots) + \frac{\triangle t}{2}(\epsilon^2\partial_{t_2} + \epsilon D_{1i})^2(f_i^{(0)} + \epsilon f_i^{(1)} + \cdots) + \cdots \\ &\quad = -\frac{1}{\tau\triangle t}(\epsilon f_i^{(1)} + \epsilon^2 f_i^{(2)} + \cdots) + \epsilon(F_i^{(1)} + G_i^{(1)} + \epsilon G_i^{(2)}) + \frac{\triangle t}{2}(\epsilon^2\partial_{t_1}F_i^{(1)} + \epsilon^3\partial_{t_2}F_i^{(1)}).\end{aligned} \tag{10}$$

Based on this equation, we can derive the equations at different orders of ϵ:

$$f_i^{(0)} = f_i^{eq}, \tag{11}$$

$$D_{1i} f_i^{(0)} = -\frac{1}{\tau\triangle t} f_i^{(1)} + F_i^{(1)} + G_i^{(1)}, \tag{12}$$

$$\partial_{t_2} f_i^{(0)} + D_{1i} f_i^{(1)} + \frac{\triangle t}{2} D_{1i}^2 f_i^{(0)} = -\frac{1}{\tau\triangle t} f_i^{(2)} + G_i^{(2)} + \frac{\triangle t}{2}\partial_{t_1} F_i^{(1)}. \tag{13}$$

From Eqs. (5), (8) and (11), we can get

$$\sum_i f_i^{(k)} = 0, \quad (k \geq 1). \tag{14}$$

Substituting Eq. (12) into Eq. (13), one can rewrite Eq. (13) in another form

$$\partial_{t_2} f_i^{eq} + D_{1i}\left(1 - \frac{1}{2\tau}\right) f_i^{(1)} + \frac{\triangle t}{2} D_{1i}(F_i^{(1)} + G_i^{(1)}) = -\frac{1}{\tau\triangle t} f_i^{(2)} + G_i^{(2)} + \frac{\triangle t}{2}\partial_{t_1} F_i^{(1)}. \tag{15}$$

Summing Eqs. (12) and (15) over i and with the help of Eqs. (5)–(7), we have

$$\partial_{t_1}\phi + \nabla_1 \cdot (a\mathbf{U}) = F^{(1)}, \tag{16}$$

$$\partial_{t_2}\phi + \nabla_1 \cdot \left[\left(1 - \frac{1}{2\tau}\right)\sum_i \mathbf{c}_i f_i^{(1)}\right] + \frac{\triangle t}{2}\nabla_1 \cdot \{\lambda[a'\mathbf{U}F^{(1)} + \mathbf{S}^{(1)}]\} = 0. \tag{17}$$

Using Eqs. (5)–(7) and (12), we can obtain

$$\begin{aligned}\sum_i \mathbf{c}_i f_i^{(1)} &= -\tau\triangle t \sum_i \mathbf{c}_i (D_{1i} f_i^{eq} - F_i^{(1)} - G_i^{(1)}) \\ &= -\tau\triangle t[\partial_{t_1}(a\mathbf{U}) + \nabla_1 \cdot (\mathbf{C} + c_s^2\beta\mathbf{D}) - \lambda a'\mathbf{U}F^{(1)} - \lambda\mathbf{S}^{(1)}].\end{aligned} \tag{18}$$

Taking $\mathbf{C} = \mathbf{U}\mathbf{U}\int a'a'd\phi$ and $\mathbf{S}^{(1)} = a\partial_{t_1}\mathbf{U} - aa'\mathbf{U}\nabla_1 \cdot \mathbf{U} + \int a'a'd\phi\nabla_1 \cdot (\mathbf{U}\mathbf{U})$, then it follows from Eqs. (16) and (18) that

$$\begin{aligned}\sum_i \mathbf{c}_i f_i^{(1)} &= -\tau\triangle t\left\{a\partial_{t_1}\mathbf{U} + \mathbf{U}a'[\partial_{t_1}\phi + \nabla_1 \cdot (a\mathbf{U}) - F^{(1)} - a\nabla_1 \cdot \mathbf{U}]\right. \\ &\quad \left. + \int a'a'd\phi\nabla_1 \cdot (\mathbf{U}\mathbf{U})\right\} - \tau\triangle t[(1-\lambda)a'\mathbf{U}F^{(1)} - \lambda\mathbf{S}^{(1)} + c_s^2\beta\nabla_1 \cdot \mathbf{D}] \\ &= -\tau\triangle t[(1-\lambda)(a'\mathbf{U}F^{(1)} + \mathbf{S}^{(1)}) + c_s^2\beta\nabla_1 \cdot \mathbf{D}].\end{aligned} \tag{19}$$

Substituting Eq. (19) into Eq. (17), we obtain

$$\partial_{t_2}\phi = \nabla_1 \cdot \left[c_s^2\left(\tau - \frac{1}{2}\right)\triangle t\beta\nabla_1 \cdot \mathbf{D}\right] + \triangle t\nabla_1 \cdot \left[\left(\tau - \frac{1}{2} - \tau\lambda\right)(\mathbf{U}a'F^{(1)} + \mathbf{S}^{(1)})\right], \tag{20}$$

with the help of $\lambda = 1 - \frac{1}{2\tau}$, Eq. (20) can be written as

$$\partial_{t_2}\phi = \nabla_1 \cdot \left[c_s^2 \left(\tau - \frac{1}{2} \right) \Delta t \beta \nabla_1 \cdot \mathbf{D} \right]. \tag{21}$$

Combining Eqs. (16), (21) and taking

$$\alpha = \beta c_s^2 \left(\tau - \frac{1}{2} \right) \Delta t, \tag{22}$$

we can derive the recovered CDE, i.e.,

$$\partial_t \phi + \nabla \cdot [a\mathbf{U}] = \nabla \cdot [\alpha \nabla \cdot \mathbf{D}] + F. \tag{23}$$

Finally, some remarks on the present model are listed as follows.

Remark 1. From the above Chapman–Enskog analysis, it is found that our model can be considered as a solver to a class of CDEs with variable coefficients in both convection and diffusion terms, and it can exactly recover CDE without any assumptions.

Remark 2. It is worth noting that when $a(\phi) = \phi$, $\mathbf{D} = \mathbf{B}\phi$ and $F = 0$, Eq. (1) becomes the following FPE [21],

$$\partial_t \phi + \nabla \cdot [\phi \mathbf{U}(\mathbf{x}, t)] = \nabla \cdot \{\nabla \cdot [\phi \mathbf{B}(\mathbf{x}, t)]\}. \tag{24}$$

Based on Eq. (4), the auxiliary distribution function can be simplified as

$$G_i = \omega_i \phi \lambda \frac{\mathbf{c}_i \cdot (\partial_t \mathbf{U} + \mathbf{U} \cdot \nabla \mathbf{U})}{c_s^2}. \tag{25}$$

Remark 3. If we exchange the scalar and vector functions in the convection term, Eq. (1) can be written as:

$$\partial_t \phi + \nabla \cdot [b(\mathbf{x}, t)\mathbf{N}(\phi)] = \nabla \cdot [\alpha(\mathbf{x}, t) \nabla \cdot \mathbf{D}(\mathbf{x}, t, \phi)] + F(\mathbf{x}, t, \phi), \tag{26}$$

which can also be solved by the present model where Eqs. (3) and (4) should be replaced by

$$\begin{aligned} f_i^{eq} &= \omega_i \left[\phi + \frac{\mathbf{c}_i \cdot (b\mathbf{N})}{c_s^2} + \frac{(\mathbf{C} + c_s^2 \beta \mathbf{D} - c_s^2 \phi \mathbf{I}) : (\mathbf{c}_i \mathbf{c}_i - c_s^2 \mathbf{I})}{2c_s^4} \right], \\ F_i &= \omega_i F \left[1 + \lambda \frac{\mathbf{c}_i \cdot (b\mathbf{N}')}{c_s^2} \right], \qquad G_i = \omega_i \lambda \frac{\mathbf{c}_i \cdot (\mathbf{N}\partial_t b - b\mathbf{N}\mathbf{N}' \cdot \nabla b + \int \mathbf{N}'\mathbf{N}' d\phi \cdot \nabla b^2)}{c_s^2}, \end{aligned} \tag{27}$$

with $\mathbf{N}' = \frac{d\mathbf{N}}{d\phi}$, $\mathbf{C} = b^2 \int \mathbf{N}'\mathbf{N}' d\phi$ and $\lambda = 1 - \frac{1}{2\tau}$. Here it should be noted that Eq. (26) is equivalent with Eq. (1) in one-dimensional space.

Remark 4. We note that although some models have been proposed for CDEs with variable coefficients, there are still some limits in these models. For instance, there are some assumptions in the model for FPE [21], including $\phi U = O(\epsilon)$ and $\phi B_{21} = O(\epsilon)$. Besides, the model in Ref. [21] can only be used for one and two dimensional FPEs. Finally, the present model can be viewed as an extension of our model in Ref. [16], where the CDE is given as: $\partial_t \phi + \nabla \cdot \mathbf{B}(\phi) = \nabla \cdot [\alpha \nabla D(\phi)] + F(\mathbf{x}, t)$.

3. Numerical simulation

In this section, some numerical simulations of six n-dimensional ($n = 1, 2, 3$) CDEs with variable coefficients were carried out to test the proposed model. To give a comparison between present model and the available one in Ref. [21], three examples in Ref. [21] are used in the present work. Besides, to further show the capacity of the present model, the three rest examples in different dimensions are also considered. In the following simulations, the non-equilibrium extrapolation scheme proposed by Guo et al. [22] is used for the boundary treatments, and an explicit difference scheme $\partial_t F_i(\mathbf{x}, t) = [F_i(\mathbf{x}, t) - F_i(\mathbf{x}, t - \Delta t)]/\Delta t$ is adopted to compute $\partial_t F_i(\mathbf{x}, t)$. The global relative error (GRE) and global maximum error (GME) are used to measure the accuracy of the present model, and defined by

$$GRE = \frac{\sum_j |\phi(\mathbf{x}_j, t) - \phi^*(\mathbf{x}_j, t)|}{\sum_j |\phi^*(\mathbf{x}_j, t)|}, \qquad GME = MAX_j |\phi(\mathbf{x}_j, t) - \phi^*(\mathbf{x}_j, t)|, \tag{28}$$

where $\phi(\mathbf{x}_j, t)$ and $\phi^*(\mathbf{x}_j, t)$ are the numerical and analytical solutions, respectively.

Table 2
Errors of different models for Example 1 at different time.

	$t = 0.5$	$t = 1.0$	$t = 1.5$	$t = 2.0$	$t = 2.5$
M1 *GRE*	8.7109×10^{-5}	4.8648×10^{-5}	2.4916×10^{-4}	1.1725×10^{-3}	1.6120×10^{-3}
M1 *GME*	4.9184×10^{-5}	1.1699×10^{-5}	5.0734×10^{-6}	1.9453×10^{-9}	1.5551×10^{-20}
M2 *GRE*	1.0544×10^{-4}	5.3256×10^{-5}	1.5099×10^{-4}	2.3173×10^{-4}	1.0560×10^{-4}
M2 *GME*	5.7019×10^{-5}	1.2130×10^{-5}	5.1711×10^{-6}	3.9371×10^{-10}	1.0645×10^{-21}
M3 *GRE*	1.0082×10^{-4}	2.6409×10^{-5}	2.8077×10^{-5}	4.2228×10^{-5}	7.9306×10^{-6}
M3 *GME*	5.4553×10^{-5}	5.9779×10^{-6}	7.9537×10^{-7}	6.5942×10^{-11}	6.6500×10^{-23}

For simplicity, to conduct a comparison between different models, we denoted the LB model in Refs. [21,16] and present model as model 1 (M1), model 2 (M2) and model 3 (M3), respectively, and without otherwise stated, the M3 is used in the following simulations. For the initial condition without the Dirac delta function, $\phi(\mathbf{x}_j, 0) = 0$ is adopted to initialize the equilibrium distribution function except for given boundary conditions, while the process of implementing the initial condition with the Dirac delta function is the same as Ref. [21], i.e., for the following initial condition,

$$\phi(\mathbf{x}, 0) = \delta(\mathbf{x} - \mathbf{X}_0) = \begin{cases} \infty, & \mathbf{x} = \mathbf{X}_0, \\ 0, & \mathbf{x} \neq \mathbf{X}_0, \end{cases}$$

and

$$\int_{-\infty}^{+\infty} \delta(\mathbf{x} - \mathbf{X}_0) = 1.$$

We have

$$\phi(\mathbf{x}_j, 0) = \begin{cases} \dfrac{1}{\Delta \mathbf{x}}, & |\mathbf{x}_j - \mathbf{X}_0| \leq \eta, \\ 0, & \text{else}, \end{cases}$$

where η is a small constant to exclude all other points x_k with $k \neq j$.

3.1. One-dimensional CDEs

Example 1. The nonlinear FPE of the Desai–Zanzing type [21]

$$\partial_t \phi + \partial_x \{[tx + \langle x(t) \rangle]\phi\} = \partial_{xx}(2t\phi), \tag{29}$$

with the initial condition $\phi(x, 0) = \delta(x - X_0)$, was first considered. The exact solution of the problem is given by

$$\phi(x, t) = \frac{1}{\sqrt{4\pi\eta(t)\exp(t^2)}} \exp\left\{-\frac{[x - \langle x(t) \rangle]^2}{4\eta(t)\exp(t^2)}\right\}, \tag{30}$$

where $\eta(t) = 1 - \exp(-t^2)$, $\langle x(t) \rangle = \exp(t + \frac{t^2}{2})$, and $X_0 = 1.0$.

We used the present model with D1Q3 lattice to solve this problem in the interval $[-2, 8]$, and took $a = \phi$, $U = tx + \exp(t + \frac{t^2}{2})$, $D = 2t\phi$, $F = 0.0$, $C = U^2\phi$, and $S = \phi[x + \langle x(t) \rangle(1 + t) + Ut]$. Fig. 1 shows a comparison between exact solutions and numerical results, where $\Delta x = 0.025$, $\Delta t = 5 \times 10^{-5}$, $\beta = 0.702$, $\phi(x, 0) = 0$ except $\phi(1, 0) = 40$ [21]. As seen from this figure, the numerical results agree well with the corresponding exact solutions.

To test the accuracy of the proposed model and conducted a comparison among different models, several simulations were performed at different lattice resolutions ($\Delta x = 1/10 - 1/160$), c was correspondingly changed from 250 to 4000, and $\beta = 0.351$. Based on the *GRE* and *GME* at time $t = 1.0$ (see Fig. 2), the slopes of the fitting lines are very close to 2, which indicates all of the three models have a second-order accuracy in space.

Furthermore, we also performed a comparison of precision between different models, and presented the results in Table 2 where $\Delta x = 0.025$, $\Delta t = 2.5 \times 10^{-5}$, $\tau = 0.842$. From Table 2, we can see that the M3 is better than the previous M1 and M2, especially at a large time and a relative large time step Δt. While we also noted that the errors of present model in first column of Table 2 are larger than other models, which may be caused by the influence of initialization error. The same as in Ref. [19], we also presented the *GRE* of three models at different parameters c and β in Table 3 where $\Delta x = 0.025$ and $t = 1.0$, and found that the present model is also better than previous M1 and M2. Based on the results presented above, we can conclude that the present model is an accurate algorithm in solving this special CDE.

Example 2. We also used another FPE [21]

$$\partial_t \phi + \partial_x [2 \tanh(x)\phi] = \partial_{xx}\phi, \tag{31}$$

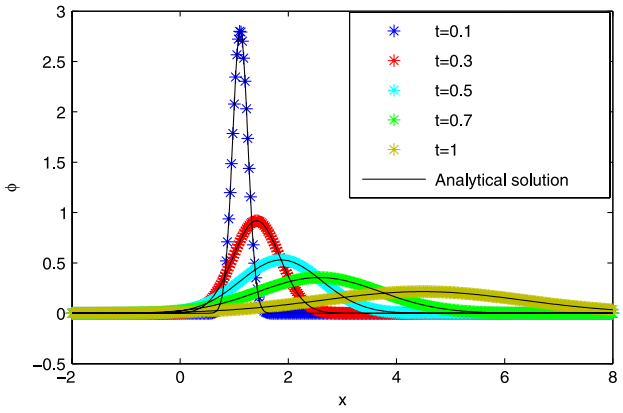

Fig. 1. Comparison of analytical solutions (solid) with numerical solutions (symbol) for Example 1 at different time.

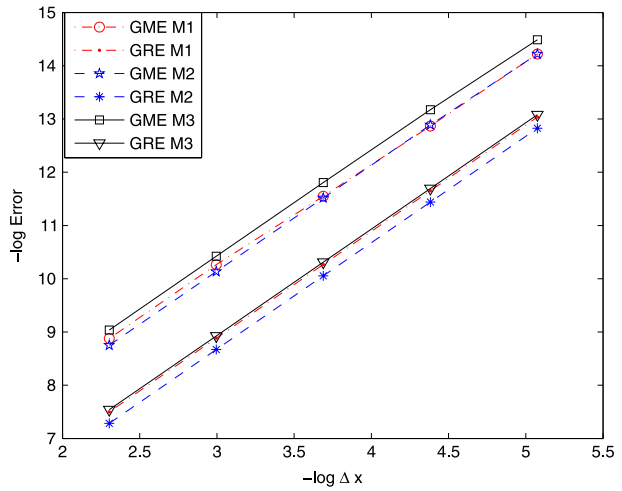

Fig. 2. Accuracy test of different models for Example 1.

Table 3
GRE for Example 1 of different models.

	β	0.7	0.701754	0.8
M1	$c = 400$	1.8430×10^{-4}	1.8328×10^{-4}	1.3786×10^{-4}
	$c = 500$	9.0676×10^{-5}	9.0018×10^{-5}	6.3487×10^{-5}
	$c = 600$	4.3657×10^{-5}	4.3330×10^{-5}	2.9473×10^{-5}
M2	$c = 400$	1.2626×10^{-4}	1.2554×10^{-4}	9.6720×10^{-5}
	$c = 500$	7.3828×10^{-5}	7.3518×10^{-5}	6.3770×10^{-5}
	$c = 600$	5.3819×10^{-5}	5.3753×10^{-5}	5.3536×10^{-5}
M3	$c = 400$	3.7124×10^{-5}	3.6431×10^{-5}	1.0981×10^{-5}
	$c = 500$	1.7459×10^{-5}	1.7598×10^{-5}	2.8407×10^{-5}
	$c = 600$	3.3226×10^{-5}	3.3439×10^{-5}	4.3032×10^{-5}

with the initial condition $\phi(\mathbf{x}, 0) = \delta(x - 0)$ to test present model. The problem has the following exact solution

$$\phi(x, t) = \frac{1}{4\sqrt{\pi t}} \left\{ \exp\left[-\left(\frac{x}{2\sqrt{t}} + \sqrt{t} \right)^2 \right] + \exp\left[-\left(-\frac{x}{2\sqrt{t}} + \sqrt{t} \right)^2 \right] \right\}. \tag{32}$$

We took $a = \phi$, $U = 2\tanh(x)$, $D = \phi$, $F = 0.0$, $C = U^2\phi$, and $S = 2\phi U(1 - \tanh^2(x))$ in the interval $[-5, 5]$, and showed the results in Fig. 3 where $\Delta x = 0.1$, $\Delta t = 1.0 \times 10^{-4}$, $\beta = 0.06$, $\phi(x, 0) = 0$ except $\phi(0, 0) = 10$. As seen from this figure, the numerical results are in good agreement with the exact solutions.

Similarly, to test the accuracy of the proposed model and performed a comparison between different models, simulations were performed at different lattice resolutions ($\Delta x = 1/10 - 1/160$), c was correspondingly varied from 75 to 600, and

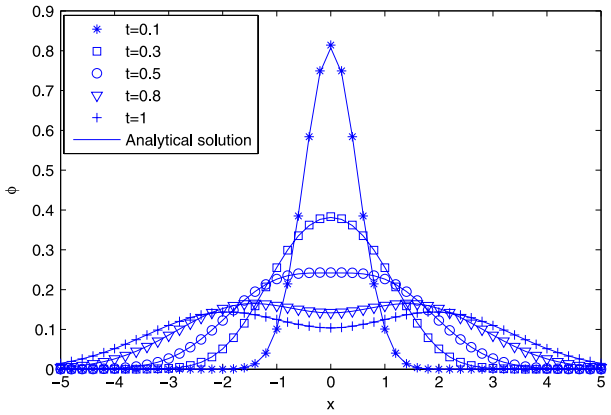

Fig. 3. Comparison between numerical solutions (symbol) and analytic results (solid) for Example 2 at different time.

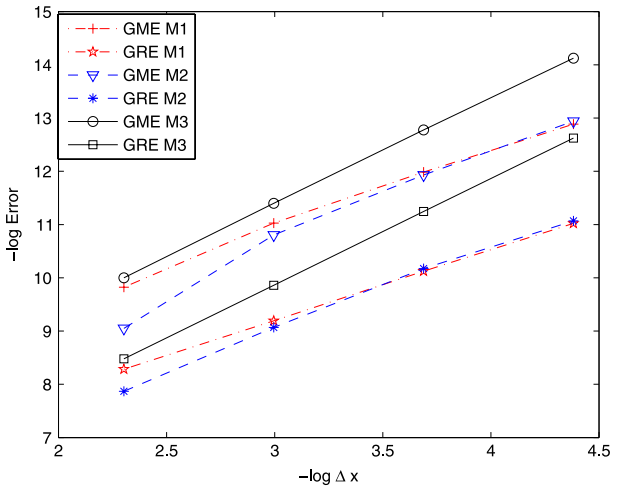

Fig. 4. Accuracy test of different models for Example 2.

Table 4
Errors of different models for Example 2 at different time.

t	$t = 0.5$	$t = 1.0$	$t = 1.5$	$t = 2.0$
M1 *GRE*	3.0540×10^{-4}	2.6696×10^{-4}	3.7935×10^{-4}	4.4226×10^{-4}
M1 *GME*	6.8714×10^{-5}	5.5293×10^{-5}	6.1135×10^{-5}	6.5802×10^{-5}
M2 *GRE*	2.6517×10^{-4}	3.9005×10^{-4}	3.7869×10^{-4}	3.5974×10^{-4}
M2 *GME*	1.1238×10^{-4}	1.2143×10^{-4}	8.0257×10^{-5}	4.9887×10^{-5}
M3 *GRE*	2.1750×10^{-4}	2.0817×10^{-4}	1.6675×10^{-4}	1.7244×10^{-4}
M3 *GME*	5.4380×10^{-5}	4.5426×10^{-5}	2.9427×10^{-5}	1.7137×10^{-5}

$\beta = 1.0$. As seen from Fig. 4, the slopes of the fitting lines for M3 results are about 1.99, while they are far from 2 for M1 and M2, which indicates that only M3 has a second-order accuracy in space for this special CDE.

In addition, we also carried out a comparison of precision between different models for the case of $\tau = 0.9$, $\Delta x = 0.1$, $\Delta t = 0.0013$, and presented the results in Table 4. To see the results more clearly, we also gave errors at different time in Fig. 5. From Table 4 and Fig. 5, it can be seen that M3 performs better than others.

Finally, we also tested the effects of parameters c and β, and presented the results in Table 5 where $\Delta x = 0.1$ and $t = 1.0$, and found that the accuracy of the present model is much better than previous models.

Example 3. The Burgers equation with variable coefficient

$$\partial_t \phi + \partial_x [x\phi^2] = \partial_{xx}\phi + x + 3x^2 t^2, \tag{33}$$

was also considered in this work. The analytical solution to this problem can be given as

$$\phi(x, t) = xt. \tag{34}$$

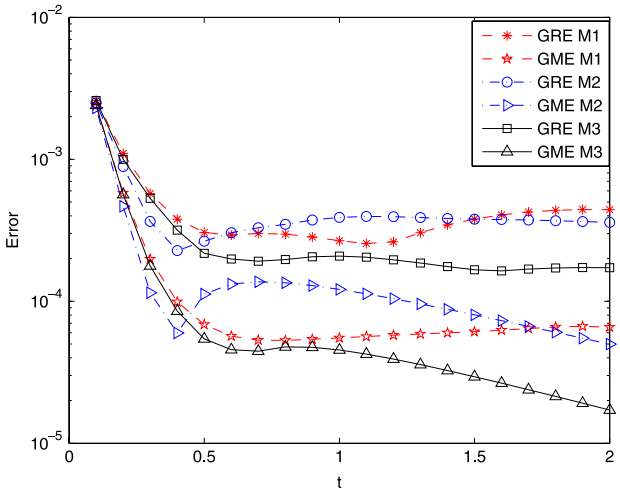

Fig. 5. Errors for Example 2 at different time.

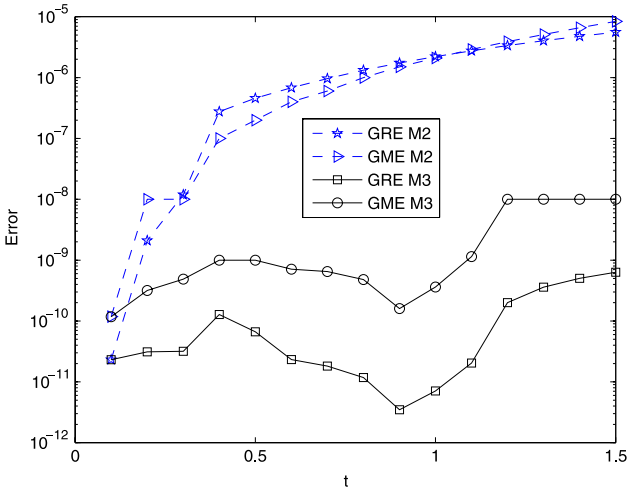

Fig. 6. Errors of different LB models (M2, 3: model 2, 3) for Example 3.

Table 5
GRE of different models for Example 2.

	β	$\beta = 0.9$	$\beta = 1.0$	$\beta = 1.1$
M1	$c = 50$	3.4359×10^{-3}	2.3508×10^{-3}	1.6076×10^{-3}
	$c = 75$	6.4097×10^{-4}	2.6696×10^{-4}	3.1400×10^{-4}
M2	$c = 50$	3.6022×10^{-3}	2.4467×10^{-3}	1.6291×10^{-3}
	$c = 75$	7.7711×10^{-4}	3.9005×10^{-4}	3.7150×10^{-4}
M3	$c = 50$	3.0133×10^{-3}	1.9125×10^{-3}	1.1381×10^{-3}
	$c = 75$	4.8941×10^{-4}	2.0817×10^{-4}	3.5100×10^{-4}

We still used the proposed model D1Q3 lattice to study this problem in the interval $[-1, 1]$, and took $a = \phi^2$, $U = x$, $D = \phi$, $F = x + 3x^2t^2$, $C = \frac{4\phi^3x^2}{3}$, $S = \frac{2\phi^3x}{3}$, $\Delta x = 0.02$, $\Delta t = 6.67 \times 10^{-5}$, $\beta = 1.0$. We presented the results in Fig. 6, and also found that M3 is better than M2.

We further performed some simulations to test the accuracy of the proposed model at different lattice resolutions ($\Delta x = 1/50 - 1/400$), c is correspondingly changed from 300 to 2400 with $\beta = 1.0$. Based on the *GRE* and *GME* shown in Fig. 7, the slopes of the fitting lines for M3 are about 4, indicating that the present model has a fourth-order accuracy in space for this problem. Furthermore, we also conducted a comparison of precision between M2 and M3, and presented the results in Table 6 where $\tau = 1.0$, $\Delta x = 0.02$, $\Delta t = 6.67 \times 10^{-5}$. From Table 6, we can see that the present model performs much better than the previous M2.

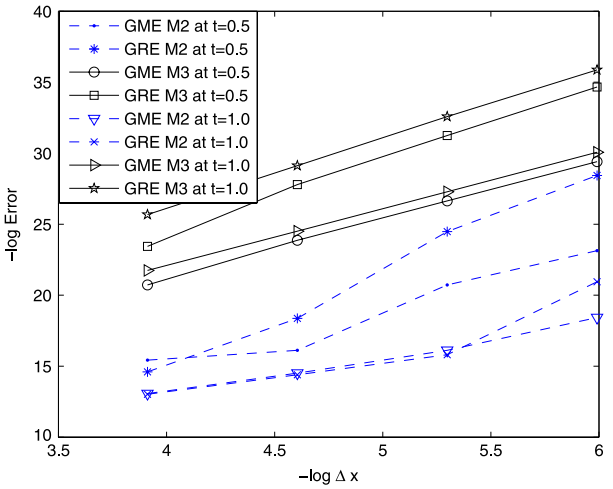

Fig. 7. Accuracy test of different models for Example 3.

Table 6
Errors of different models for Example 3 at different time.

t	M2		M3	
	GRE	*GME*	*GRE*	*GME*
1	2.2173×10^{-6}	2.1000×10^{-6}	7.0887×10^{-12}	3.6152×10^{-10}
2	1.1161×10^{-5}	2.3000×10^{-5}	2.4371×10^{-8}	1.0000×10^{-7}
3	3.1521×10^{-5}	1.0400×10^{-4}	1.1628×10^{-7}	1.0000×10^{-6}
4	6.9980×10^{-5}	3.1500×10^{-4}	2.8262×10^{-7}	2.0000×10^{-6}
5	1.3211×10^{-4}	7.5800×10^{-4}	5.6200×10^{-7}	4.0000×10^{-6}
6	2.2009×10^{-4}	1.5440×10^{-3}	9.1835×10^{-7}	7.0000×10^{-6}
7	3.3225×10^{-4}	2.7750×10^{-3}	1.3968×10^{-6}	1.3000×10^{-5}
8	4.6419×10^{-4}	4.5230×10^{-3}	1.9222×10^{-6}	2.0000×10^{-5}
9	6.1089×10^{-4}	6.8410×10^{-3}	2.5064×10^{-6}	3.0000×10^{-5}
10	7.6821×10^{-4}	9.7570×10^{-3}	3.1257×10^{-6}	4.2000×10^{-5}

3.2. Two-dimensional CDEs

Example 4. We also used 2D FPE [21]

$$\partial_t \phi + \partial_x \left(\frac{4\phi^2}{x} \right) + \partial_y (y\phi) = \partial_{xx}(\phi^2) + 2\partial_{xy}\phi + \partial_{yy}(\phi^2), \tag{35}$$

to test present model. The problem has the following exact solution

$$\phi(x, t) = x^2 \exp(-t). \tag{36}$$

The present model with D2Q9 lattice was applied to solve this problem on the domain $[1, 6] \times [1, 6]$, and the results at $y = 3.0$ and different time were presented in Fig. 8 where $a = \phi$, $\mathbf{U} = (\frac{4\phi}{x}, y)^T$, $\mathbf{D} = \begin{pmatrix} \phi^2 & \phi \\ \phi & \phi^2 \end{pmatrix}$, $\Delta x = \Delta y = 0.1$, $\Delta t = 1.0 \times 10^{-5}$, $\beta = 0.006$. As seen from this figure, the numerical results are in good agreement with the exact solutions.

Similar to above discussion, to test the accuracy of the proposed model for this special two-dimensional problem, some simulations were conducted under different lattice resolutions ($\Delta x = 1/100 - 1/800$), c was correspondingly changed from 500 to 4000, and $\beta = 0.012$. Based on the results of *GRE* and *GME* at time $t = 0.5$ (see Fig. 9), one can found that the slopes of the fitting lines for different models are close to 2, indicating that all of the three models have a second-order convergence rate in space. Besides, we also presented errors at different time in Fig. 10 where $\Delta x = \Delta y = 0.1$, $\Delta t = 2 \times 10^{-5}$, $\tau = 1$, and found that the present model is better that previous M1 and M2 for this two-dimensional FPE. The little difference between these models may be due to relatively small $\Delta t = 2 \times 10^{-5}$ and the weak convection term.

Example 5. The 2D CDE with variable coefficients

$$\partial_t \phi + \partial_x (10x\phi) + \partial_y (10y\phi) = \partial_{xx}\phi + \partial_{yy}\phi + [10(x + y) + 19]\phi, \tag{37}$$

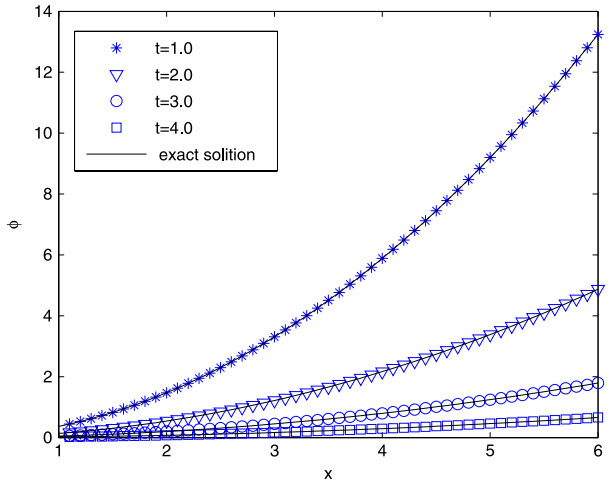

Fig. 8. Comparison between numerical solutions (symbol) and analytic results (solid) for Example 4 at different time.

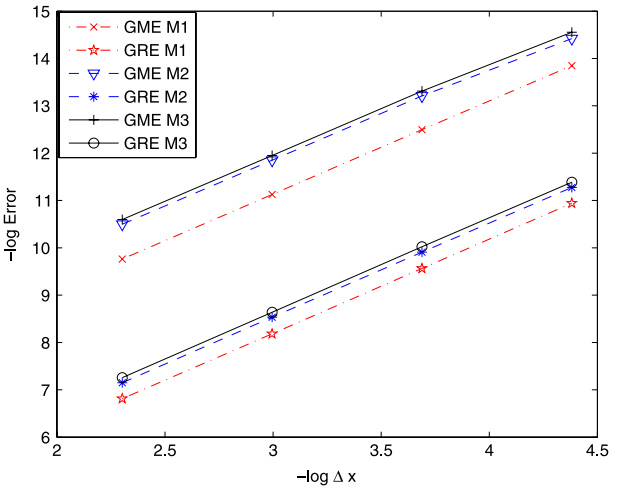

Fig. 9. Accuracy test of different models for Example 4.

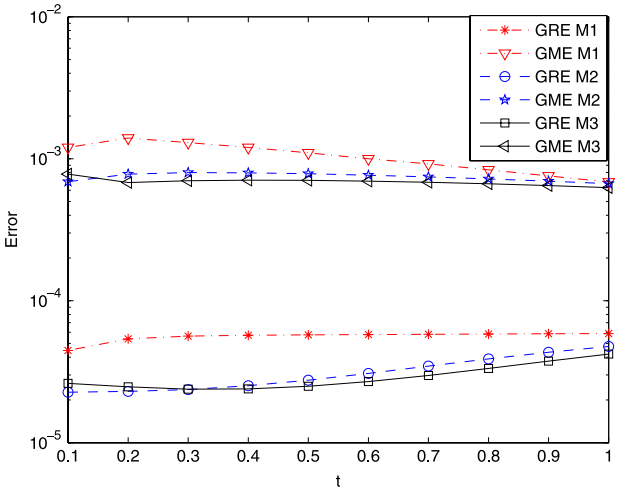

Fig. 10. Errors of different models for Example 4 at different time.

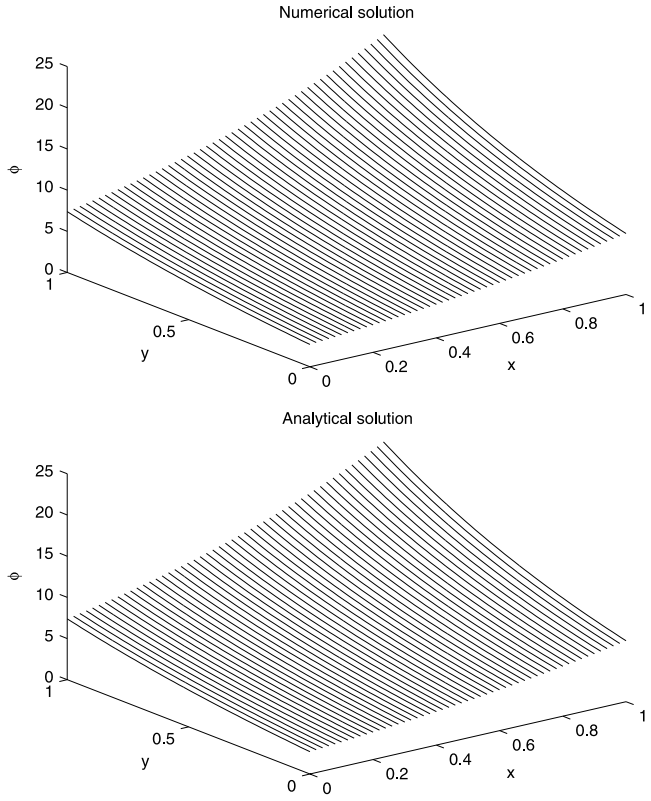

Fig. 11. Comparison between analytical solution and numerical result for Example 5 at time $t = 1.0$.

Table 7
Errors of different models for Example 5 at different time [MAX: global maximum].

t	M2		M3	
	GRE	*GME/MAX*	*GRE*	*GME/MAX*
1	0.0044	0.0044	7.1015×10^{-4}	0.0020
2	0.0050	0.0049	7.3467×10^{-4}	0.0029
3	0.0053	0.0051	8.1971×10^{-4}	0.0033
4	0.0053	0.0052	8.6191×10^{-4}	0.0034
5	0.0054	0.0052	8.7909×10^{-4}	0.0034
6	0.0054	0.0053	8.8563×10^{-4}	0.0035
7	0.0054	0.0053	8.8805×10^{-4}	0.0035
8	0.0054	0.0053	8.8894×10^{-4}	0.0035
9	0.0054	0.0053	8.8927×10^{-4}	0.0035
10	0.0054	0.0053	8.8939×10^{-4}	0.0035
100	0.0054	0.0053	8.8947×10^{-4}	0.0035

was further considered. The exact solution of this problem is given by $\phi(x, y, t) = \exp(x + y + t)$. We adopted the present model with D2Q9 lattice to study this problem in the domain $[0, 1] \times [0, 1]$, and took $a = \phi$, $\mathbf{U} = 10(x, y)^T$, $\mathbf{D} = \phi\mathbf{I}$, $F = \phi[10(x + y) + 19]$, $\mathbf{C}_{\alpha\beta} = \phi\mathbf{U}_\alpha\mathbf{U}_\beta$, $\mathbf{S} = 100\phi(x, y)^T$, $\Delta x = 0.02$, $\Delta t = 2.0 \times 10^{-4}$ and $\beta = 3.0$. We presented the results in Fig. 11, and found that the numerical result agrees well with the analytic solution, and the global relative error is $GRE = 7.8733 \times 10^{-4}$.

Furthermore, we also studied the precision between different models, and presented the results in Table 7 where $\tau = 2.0$, $\Delta x = 0.02$, $\Delta t = 2 \times 10^{-4}$ at different time. Besides that, we also investigated the effect of parameters c and β under $\Delta x = \Delta y = 0.02$, and presented *GREs* at time $t = 1.0$ in Table 8. From Tables 7 and 8, one can see that the accuracy of the present model is much better than the previous model M2. To test the accuracy of the proposed model, simulations were also carried out at different lattice resolutions ($\Delta x = 1/50 - 1/400$), c was changed from 300 to 2400 with $\beta = 1.0$. As shown in Fig. 12, although the slopes of the fitting lines are about 2, indicating both models have a second-order accuracy in space, the present model is more accurate in solving this two-dimensional problem.

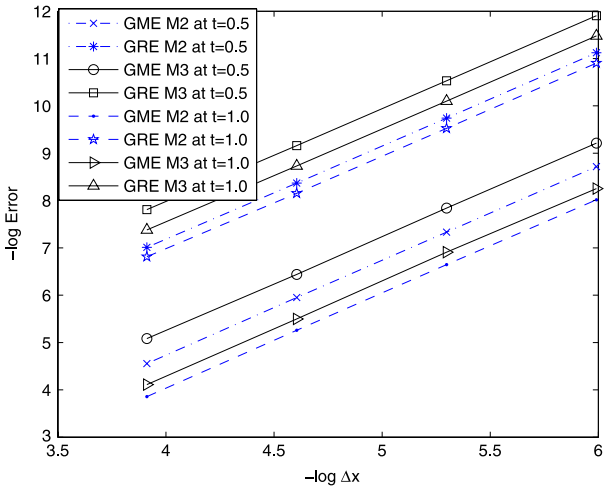

Fig. 12. Accuracy test of different models for Example 5.

Table 8
GREs of different models for Example 5 ('Blanks': divergent).

	β	$\beta = 0.8$	$\beta = 1.0$	$\beta = 3.0$
M2	$c = 100$	4.5754×10^{-3}	4.3821×10^{-3}	2.2723×10^{-3}
	$c = 200$	1.8456×10^{-3}	1.7165×10^{-3}	
	$c = 300$	1.2184×10^{-3}	1.1194×10^{-3}	
M3	$c = 100$	1.6285×10^{-3}	7.1015×10^{-4}	7.8733×10^{-4}
	$c = 200$	4.3420×10^{-4}	5.9350×10^{-4}	
	$c = 300$	5.9655×10^{-4}	6.2364×10^{-4}	

3.3. Three-dimensional CDE

Example 6. The 3D CDE

$$\partial_t \phi + \partial_x(10x\phi) + \partial_y(10y\phi) + \partial_z(10z\phi) = \partial_{xx}\phi + \partial_{yy}\phi + \partial_{zz}\phi + [10(x + y + z) + 28]\phi, \tag{38}$$

with following exact solution

$$\phi(x, y, z, t) = \exp(x + y + z + t), \tag{39}$$

was also adopted to test the present model. We took $a = \phi$, $\mathbf{U} = 10(x, y, z)^T$, $\mathbf{D} = \phi\mathbf{I}$, $F = \phi[10(x + y + z) + 28]$, $\mathbf{C}_{\alpha\beta} = \phi\mathbf{U}_\alpha\mathbf{U}_\beta$, $\mathbf{S} = 100\phi(x, y, z)^T$, and applied the present model with D3Q*15* and D3Q*19* lattices to solve this problem in the domain $[0, 1] \times [0, 1] \times [0, 1]$. We tested the accuracies of different models for this three-dimensional problem, and presented errors at different lattice resolutions in Fig. 13, where $\beta = 1.5$ and $t = 0.5$, c was changed from 100 to 600. Based on the *GRE* and *GME* shown in Fig. 13, one can found that all slopes of the fitting lines are close to 2, which indicates both models have a second-order accuracy in space.

In addition, we also compared the precision between different models, and presented the results at different time in Table 9 where $\tau = 2.0$, $\Delta x = 0.02$, $\Delta t = 2 \times 10^{-4}$. Similarly, we also presented *GREs* of two models at different parameters c and β in Table 10 where $\Delta x = \Delta y = \Delta z = 0.02$ and $t = 1.0$. From Table 10, one can found that the accuracy of M3 is much better than M2, especially at a relatively large Δt or small c, i.e. when $c = 100$, the error of M2 is three times larger than M3, while for the case of $c = 300$, the error of M2 is only a little less than that of M3. From the results shown above, we can also concluded that the present model is accurate and efficient in solving this special three-dimensional CDE.

4. Conclusion

A LBGK model for the CDE with variable coefficients in the convection and diffusion terms is proposed by introducing an auxiliary distribution function. The present model is an extension of the models in Refs.[16,21], and can exactly recover CDE without any assumptions. A detailed numerical study on six n-dimensional ($n = 1, 2, 3$) CDEs, including the FPE, Burgers equation and some others, is performed to validate the present model, and the numerical results show that the present model is better than the previous models. Actually, in the practical applications, the velocity $\mathbf{U}$ is usually not a constant, like the heat and mass transfer in fluid flows, therefore, the present model may be more useful in the study of such problems.

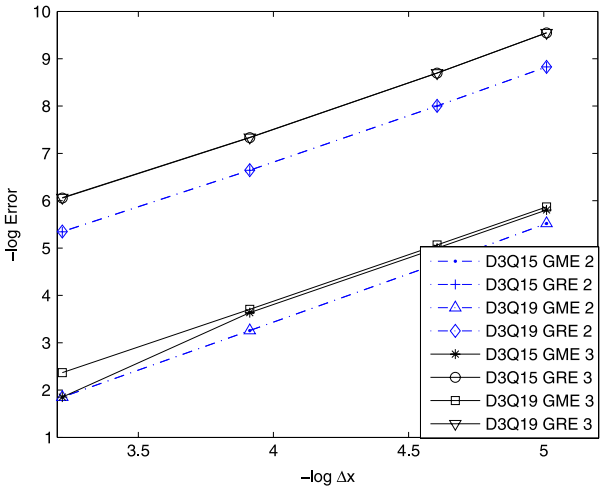

Fig. 13. Accuracy test of different models for Example 6.

Table 9
GREs of different models for Example 6 at different time.

t	M2		M3	
	D3Q15	D3Q19	D3Q15	D3Q19
1	1.6196×10^{-3}	1.6156×10^{-3}	9.7074×10^{-4}	9.6690×10^{-4}
2	1.6196×10^{-3}	1.6156×10^{-3}	9.7074×10^{-4}	9.6690×10^{-4}
3	1.6196×10^{-3}	1.6156×10^{-3}	9.7074×10^{-4}	9.6690×10^{-4}
5	1.6196×10^{-3}	1.6156×10^{-3}	9.7074×10^{-4}	9.6690×10^{-4}
10	1.6196×10^{-3}	1.6156×10^{-3}	9.7074×10^{-4}	9.6690×10^{-4}

Table 10
GREs of different models for Example 6.

		β	$\beta = 0.8$	$\beta = 1.0$	$\beta = 1.5$
M2	D3Q15	$c = 100$	4.8678×10^{-3}	4.7215×10^{-3}	3.8987×10^{-3}
		$c = 200$	2.1755×10^{-3}	2.0091×10^{-3}	1.6196×10^{-3}
		$c = 300$	1.4886×10^{-3}	1.3474×10^{-3}	1.0841×10^{-3}
	D3Q19	$c = 100$	4.8954×10^{-3}	4.6726×10^{-3}	3.8454×10^{-3}
		$c = 200$	2.1927×10^{-3}	2.0066×10^{-3}	1.6156×10^{-3}
		$c = 300$	1.4947×10^{-3}	1.3472×10^{-3}	1.0862×10^{-3}
M3	D3Q15	$c = 100$	1.5232×10^{-3}	9.2038×10^{-4}	1.2443×10^{-3}
		$c = 200$	9.3794×10^{-4}	1.0256×10^{-3}	9.7074×10^{-4}
		$c = 300$	9.4524×10^{-4}	9.1477×10^{-4}	7.8970×10^{-4}
	D3Q19	$c = 100$	1.5456×10^{-3}	9.1986×10^{-4}	1.1976×10^{-3}
		$c = 200$	9.5281×10^{-4}	1.0231×10^{-3}	9.6690×10^{-4}
		$c = 300$	9.5107×10^{-4}	9.1453×10^{-4}	7.9990×10^{-4}

Acknowledgment

This study is supported by the National Natural Science Foundation of China (Grant Nos. 11272132, 51006040).

References

[1] H. Brezis, F. Browder, Partial differential equations in the 20th century, Adv. Math. 135 (1998) 76–144.
[2] A.M. Wazwaz, Partial Differential Equations Methods and Applications, Balkema, Netherlands, 2002.
[3] B. Cockburn, C.W. Shu, The lacal difcontinuous Galerkin method for time-dependent convection–diffusion systems, SIAM J. Numer. Anal. 35 (1998) 2440–2463.
[4] B.R. Baligaa, S.V. Patanka, A new finite-element formulation for convection–diffusion problems, Numer. Heat Transfer 3 (1980) 393–409.
[5] M.M. Gupta, R.P. Manohar, J.W. Stephenson, A single cell high order scheme for the convection–diffusion equation with variable coefficients, Int. J. Numer. Methods Fluids 4 (1984) 641–651.
[6] J.C. Kalita, D.C. Dalal, A.K. Dass, A class of higher order compact schemes for the unsteady two-dimensional convectionCdiffusion equation with variable convection coefficients, Int. J. Numer. Methods Fluids 38 (2002) 1111–1131.
[7] O. Angelini, K. Brenner, D. Hilhorst, A finite volume method on general meshes for a degenerate parabolic convection-reaction–diffusion equation, Numer. Math. 123 (2013) 219–257.

[8] R. Benzi, S. Succi, M. Vergassola, The lattice Boltzmann equation: theory and applications, Phys. Rep. 222 (1992) 145–197.
[9] J.F. Zhang, Lattice Boltzmann method for microfluidics: models and applications, Microfluid. Nanofluid. 10 (2011) 1–28.
[10] T. Inamuro, T. Ogata, S. Tajima, N. Konishi, A lattice Boltzmann method for imcompressible two-phase flows with large density differences, J. Comput. Phys. 198 (2004) 628–644.
[11] M.R. Swift, E. Orlandini, W.R. Osborn, J.M. Yeomans, Lattice Boltzmann simulations of liquid-gas and binary fluid systems, Phys. Rev. E 54 (1996) 5041.
[12] F.J. Alexander, S. Chen, J.D. Sterling, Lattice Boltzmann thermohydrodynamics, Phys. Rev. E 47 (1993) R2249.
[13] Z.H. Chai, B.C. Shi, Simulation of electro-osmotic flow in microchannel with lattice Boltzmann method, Phys. Lett. A 364 (2007) 183–188.
[14] S.P. Dawson, S. Chen, G.D. Doolen, Lattice Boltzmann computations for reaction–diffusion equations, J. Chem. Phys. 98 (1993) 1514–1523.
[15] B. Chopard, J.L. Falcone, J. Latt, The lattice Boltzmann advection–diffusion model revisited, Eur. Phys. J. Spec. Top. 171 (2009) 245–249.
[16] B.C. Shi, Z.L. Guo, Lattice Boltzmann model for nonlinear convection–diffusion equations, Phys. Rev. E 79 (2009) 016701.
[17] I. Ginzburg, Equilibrium-type and link-type lattice Boltzmann models for generic advection and anisotropic-dispersion equation, Adv. Water Resour. 28 (2005) 1171–1195.
[18] Z.H. Chai, T.S. Zhao, Lattice Boltzmann model for the convection–diffusion equation, Phys. Rev. E 87 (2013) 063309.
[19] X.Q. Xiang, Z.H. Wang, B.C. Shi, Modified lattice Boltzmann scheme for nonlinear convection diffusion equations, Int. J. Nonlinear Sci. Numer. Simul. 17 (2012) 2415–2425.
[20] B.C. Shi, N.Z. He, Z.L. Guo, Lattice Boltzmann model for high-order nonlinear partial differential equations, Phys. Comp. 10 (2009).
[21] F.F. Wu, W.P. Shi, F. Liu, A lattice Boltzmann model for the Fokker–Planck equation, Commun. Nonlinear Sci. Numer. Simul. 17 (2012) 2776–2790.
[22] Z.L. Guo, C.G. Zheng, B.C. Shi, Non-equilibrium extrapolation method for velocity and pressure boundary conditionsin the lattice Boltzmann method, Chin. Phys. 11 (2002) 366–374.